Acta Crystallographica Section A
Foundations of Crystallography
ISSN 0108-7673

Received 25 June 2007
Accepted 13 November 2007

Solving the crystal structures of zeolites using electron diffraction data. II. Density-building functions

Christopher J. Gilmore,[a]* Wei Dong[a]‡ and Douglas L. Dorset[b]

[a]WestCHEM, Department of Chemistry, University of Glasgow, Glasgow G12 8QQ, Scotland, and [b]Advanced Characterization, ExxonMobil Research and Engineering Co., 1545 Route 22 East, Annandale, NJ 08801, USA. Correspondence e-mail: chris@chem.gla.ac.uk

A density-building function is used to solve the crystal structures of zeolites from electron diffraction data using both two- and three-dimensional data sets. The observed data are normalized to give unitary structure factors $|U_{\mathbf{h}}|^{\rm obs}$. An origin is defined using one to three reflections and a corresponding maximum-entropy map, $q^{\rm ME}(\mathbf{x})$, is calculated in which the constraints are the amplitudes and phases of the origin-defining reflections. Eight strong reflections are then given permuted phases and each phase combination is used to compute $P(\delta q) = \int_V \delta q\,(\mathbf{x})^2/q^{\rm ME}(\mathbf{x})\,{\rm d}\mathbf{x}$, where $\delta q(\mathbf{x})$ is the Fourier transform of $|U_{\mathbf{h}}|^{\rm obs}\exp(i\varphi_{\mathbf{h}}^{\rm perm}) - |U_{\mathbf{h}}|^{\rm ME}\exp(i\varphi_{\mathbf{h}}^{\rm ME})$, $\varphi_{\mathbf{h}}^{\rm perm}$ is the permuted phase for reflection $\mathbf{h}$ and $\varphi_{\mathbf{h}}^{\rm ME}$ is the phase angle for reflection $\mathbf{h}$ predicted from the Fourier transform of $q^{\rm ME}(\mathbf{x})$. The 64 phase sets with minimum values of $P(\delta q)$ are subjected to entropy maximization and, following this procedure, those with the five highest log-likelihood gains are examined. Sometimes auxiliary potential histogram information is also used. The method worked routinely with seven zeolite structures of varying complexity and data quality, but failed with an eighth structure.

1. Introduction and methodology

In our previous paper (Gilmore *et al.*, 2008, subsequently called GDD), we have shown how the use of potential-density histograms can be used in conjunction with entropy maximization and likelihood to solve zeolite structures from electron diffraction data with considerable success. Here we use a different method based on density-building functions combined with low-resolution maps.

The density-building methodology (Bricogne, 1984; Henderson & Gilmore, 1989; Bricogne & Gilmore, 1990; Gilmore *et al.*, 1990, 1991) works as follows.

1. The intensities of the measured reflections are normalized using Wilson's method to give $|U_h|^{\rm obs} = |E_h|^{\rm obs}/\sqrt{N}$ and the associated standard uncertainty $\sigma(|U_{\mathbf{h}}|^{\rm obs})$. N is the number of atoms, assumed equal and excluding O atoms, in the unit cell. Where possible, no overall temperature factor is imposed on the normalization. The O atoms are not located using this electron diffraction (ED) data and so are not included in any of the calculations.

2. A starting map is defined. This can come from a number of possible sources: it can be an origin map defined from one to three reflections (up to four if the enantiomorph is to be defined) in the usual way [see Rogers (1980) for a summary of the method and the necessary rules for origin definition] or a map derived from the early stages of a phase determination (Gilmore *et al.*, 1990, 1993) or an image-derived map from electron microscopy.

3. A maximum-entropy map, $q^{\rm ME}(\mathbf{x})$, is generated by maximizing the map entropy subject to the constraints of the phase and intensities of the reflections used to generate the starting map.

4. A set of reflections is now chosen which optimally enlarges the second neighbourhood of the origin and their phases are permuted using a full factorial design (*i.e.* every possible combination of phases is explored). Each permutation gives rise to a map $\delta q(\mathbf{x})$ which is the Fourier transform of

$$|U_{\mathbf{h}}|^{\rm obs}\exp(i\varphi_{\mathbf{h}}^{\rm perm}) - |U_{\mathbf{h}}|^{\rm ME}\exp(i\varphi_{\mathbf{h}}^{\rm ME}), \qquad (1)$$

where $\varphi_{\mathbf{h}}^{\rm perm}$ is the phase angle for reflection $\mathbf{h}$ generated by phase permutation and $\varphi_{\mathbf{h}}^{\rm ME}$ is the equivalent extrapolated phase from the current $q^{\rm ME}(\mathbf{x})$.

5. We now compute

$$P(\delta q) = \int_V \frac{\delta q(\mathbf{x})^2}{q^{\rm ME}(\mathbf{x})}\,{\rm d}\mathbf{x} \qquad (2)$$

for each phase permutation. A minimum value of $P(\delta q)$ is expected for the correct phase set. In practice, the 50–100 phase sets with the minimum values of $P(\delta q)$ are retained, and

‡ Present address: Cambridge Crystallographic Data Centre, 12 Union Road, Cambridge CB2 1EZ, England.

Table 1
The eight reflections given permuted phase values in the calculation of $P(\delta q)$ in the solution of the structure of mordenite.

Reflection No.	h	k	$\|U\|^{obs}$
1	2	0	0.372
2	0	8	0.317
3	6	0	0.302
4	0	10	0.239
8	0	2	0.196
12	0	6	0.122
14	0	4	0.109
16	5	3	0.097

these sets are subjected to constrained entropy maximization in the usual way with associated likelihood estimation. The *EXTEND* module in the *MICE* computer program (Gilmore & Bricogne, 1997) performs the necessary calculations. Centroid maps (see GDD) are then generated for the five to ten nodes with the largest log-likelihood gain (LLG) and inspected.

This technique has several important features:

(i) each phase permutation requires only one Fourier synthesis and a map division and so density building is very fast;

(ii) it acts as a filter to exponential modelling; the reflections to be permuted are first subjected to this filter and only those with a certain minimum $P(\delta q)$ are passed to the maximum-entropy step;

(iii) The likelihood function uses only moduli, but $P(\delta q)$ incorporates phases into the calculation. It therefore acts as a useful tool in exploring structure-factor space from the current state of knowledge before moving to various P minima.

$P(\delta q)$ cannot be used indiscriminately, there are certain necessary conditions for its successful implementation.

1. $q^{ME}(\mathbf{x})$ must have developed sufficient detail. Thus maps based on a very small basis set or utilizing only small U magnitudes may have insufficient contrast for its successful use. This is made manifest by a set of $P(\delta q)$ values that are virtually constant through phase permutation. In addition, division by $q^{ME}(\mathbf{x})$ is inherently unstable because of very low values of q and constraints in division must be employed.

2. The reflections which act as coefficients for permutation should be chosen using the same criteria of optimum second-neighbourhood extension used in regular entropy maximization. It is also advantageous to choose reflections for which there is a small but finite extrapolated magnitude from the current $q^{ME}(\mathbf{x})$.

3. Situations where there is no clear minimum or where all the $P(\delta q)$ values are constant are clear indications that either $q^{ME}(\mathbf{x})$ has insufficient contrast or that unsuitable reflections have been chosen as coefficients.

The technique preferentially selects those phases that build density where it is already well defined. This is very appropriate in this situation where we have a clear envelope. It does, however, need to be used with care as will be described later.

The method has already been used, albeit not extensively, with regard to small-molecule single-crystal diffraction (Gilmore *et al.*, 1990), powder diffraction in the solution of the crystal structure of $KAlP_2O_7$ (Gilmore *et al.*, 1993) and on studies in which protein density is built onto a low-resolution envelope using the Golay code (Golay, 1949) as a source of phase permutation (Tate, 2003). We will now modify it for use with zeolite electron diffraction data.

2. Applications to zeolite ED data

Although these zeolite data sets are difficult to solve, the cell contents are relatively small, especially as we only consider the Si T-sites. As a consequence, the U magnitudes are large (typically the largest are > 0.2), and maps based only on origin-defining reflections display considerable contrast. It is therefore possible to use such $q^{ME}(\mathbf{x})$ maps in $P(\delta q)$ calculations. Using this information coupled with pilot tests, we have established the following simple protocol.

1. Normalize using only the Si atoms in the cell contents. The O atoms contribute less than 20% to the scattering and are not usually found by direct methods. Their coordinates need to be either inferred from the Si atoms or found by subsequent crystallographic calculations based on difference density maps.

2. Define the origin and use these reflections to generate a maximum-entropy map, $q^{ME}(\mathbf{x})$. The rules initially developed by Haupman and Karle (as reviewed by Rogers, 1980) are used.

3. Select eight reflections using the criterion of optimal second-neighbourhood enhancement (Gilmore *et al.*, 1990) and compute $P(\delta q)$ for each possible phase combination. All the data sets we are using come from centrosymmetric space groups with phase angles restricted to either 0 or π and so this generates $2^8 = 256$ possible phase sets.

4. Those 64 sets having a minimum value of $P(\delta q)$ are kept and subject to constrained entropy maximization. The associated LLG is calculated for each member of the set. Each of these sets is subsequently referred to as a node.

5. It is not possible to use the scoring procedure that we usually use with maximum-entropy (ME) methods (Shankland *et al.*, 1993) because the phase space, having been filtered by $P(\delta q)$, is not evenly sampled so the nodes are sorted on LLG value and the potential centroid maps for the top five are investigated.

6. If these maps are not interpretable then potential density histograms are used (as described in the previous paper) to extend the search space.

3. Examples

We now apply this method to eight data sets. These are the same as those described in the previous paper (GDD) and the reader should refer to Table 1 of that paper for a full description of the data. However, the order in which the results are presented is different, the reasons for which will become obvious.

3.1. Mordenite

Mordenite (Meier, 1961) crystallizes in space group *Cmcm* and the data comprise 27 *hk*0 reflections with a maximum resolution of *ca* 2 Å. We will describe this first trial in detail; others will be described only briefly since they follow the same procedure. The overall temperature factor from normalization was 11.1 Å^2.

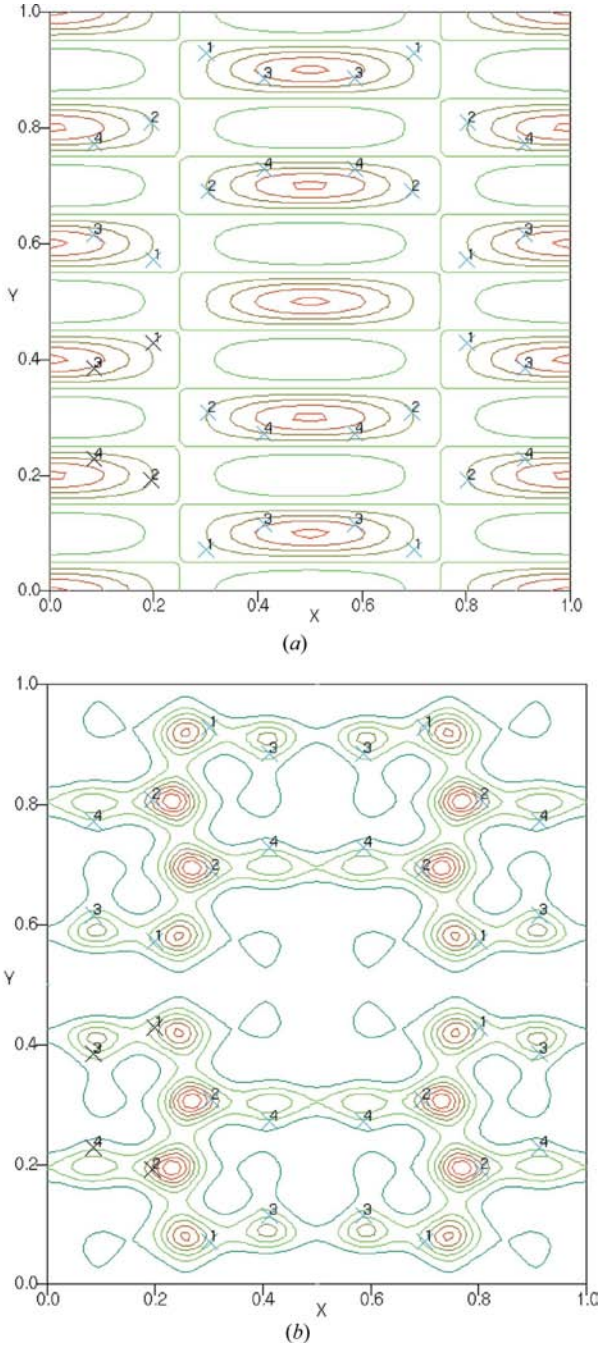

Figure 1
(*a*) Origin centroid map for mordenite based on a single reflection, 150, with $|U_{\mathbf{h}}|^{\rm obs}$ = 0.22 and phase angle 0 as constraints. The Si sites are indicated with crosses. (*b*) The centroid map for mordenite based on the origin-defined reflection and eight reflections with permuted phases filtered *via* the $P(\delta q)$ function. This is the map corresponding to the solution with the highest associated likelihood.

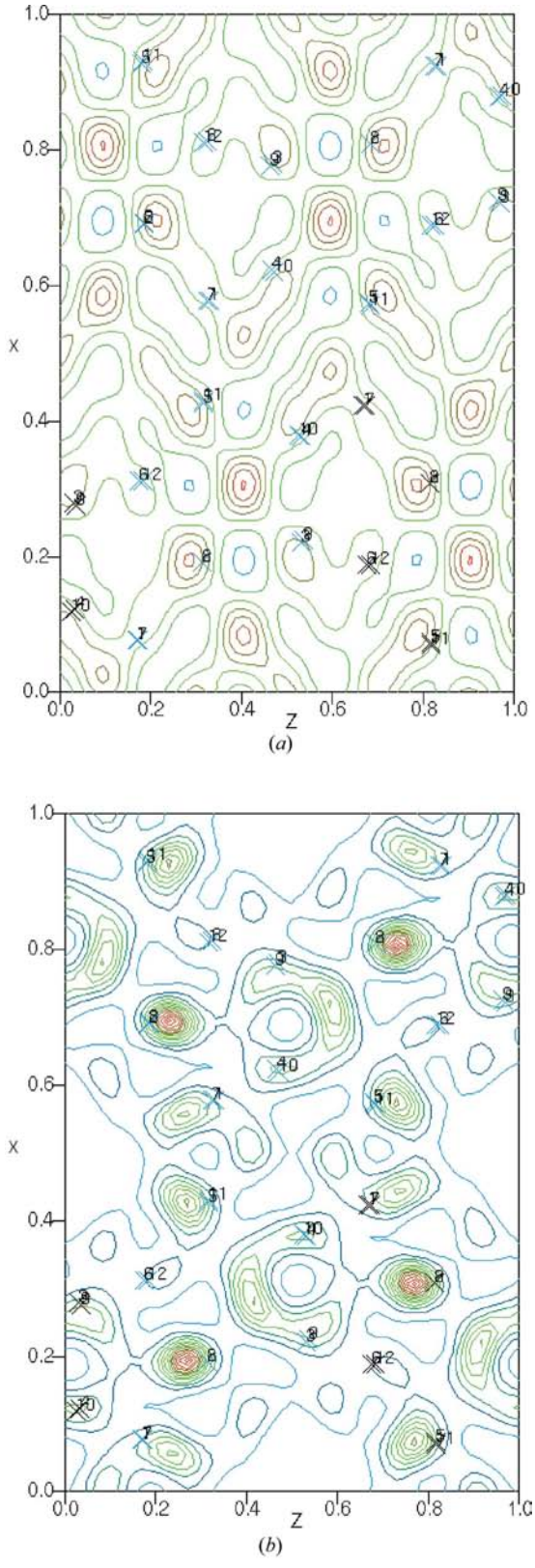

Figure 2
(*a*) Origin centroid map for ZSM-5 based on two reflections, 403, with $|U_{\mathbf{h}}|^{\rm obs}$ = 0.097, $\varphi = \pi$, and 503 with $|U_{\mathbf{h}}|^{\rm obs}$ = 0.16, φ = 0. The Si sites are indicated with crosses. (*b*) The centroid map for ZSM-5 based on the origin-defined reflections and eight reflections with permuted phases filtered *via* the $P(\delta q)$ function. This is the map with the highest associated likelihood.

The origin was defined *via* a single reflection, 150, with $|U_{\mathbf{h}}|^{\rm obs} = 0.22$ as required by the plane group, and assigned a phase angle 0 corresponding to the angle from the refined crystal structure. As in the previous paper, we will always use phase angles for origin definition calculated from the known crystal structure. This choice in no way invalidates the calculations: it simply ensures that the maps and atomic coordinates all have the same origin as the published ones. Table 1 lists the reflections that were used. The resulting maximum-entropy map is shown in Fig. 1(*a*). It can be seen that much of the density correctly defines a low-resolution molecular envelope apart from the ellipse centred on (0.5,0.5). There is sufficient dynamic range in the map for the $P(\delta q)$ formalism to work. Table 1 lists the reflections that were given permuted phases in a full factorial design.

The $P(\delta q)$ function was calculated for each of the $2^8 = 256$ phase combinations. The 64 phase sets with the minimum associated values of this function were retained and subjected to entropy maximization. The resulting likelihood estimates

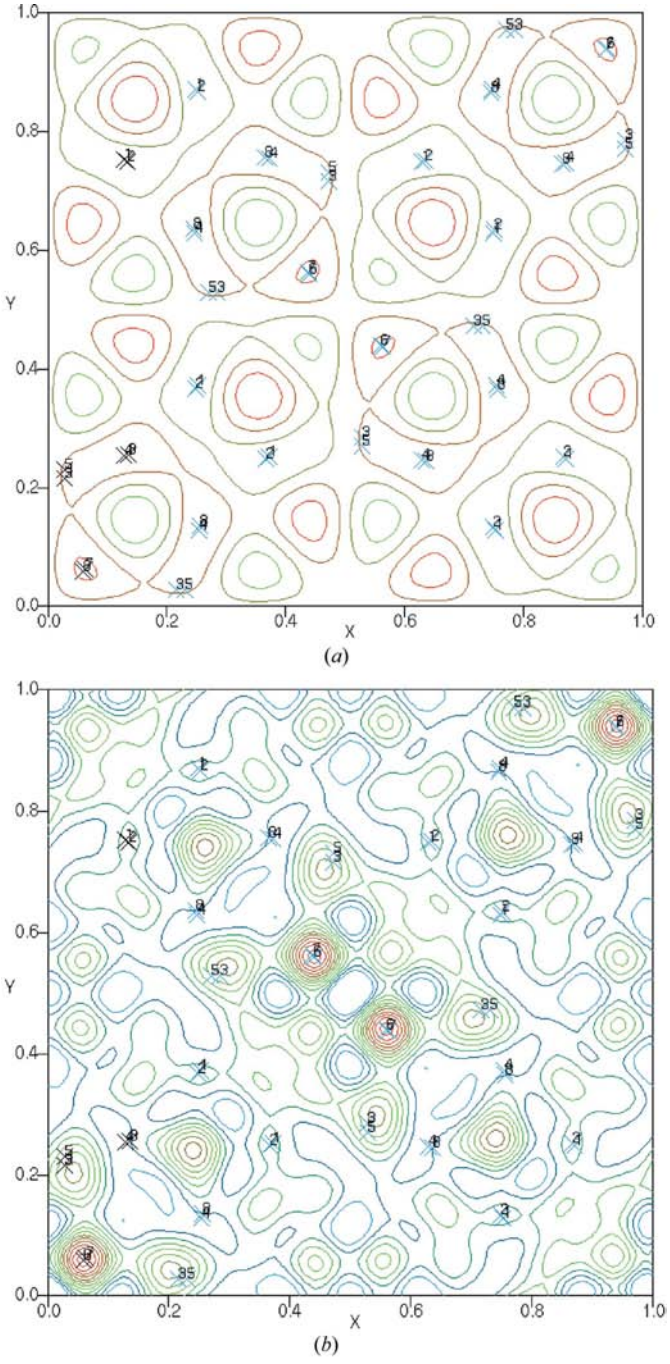

Figure 3
(*a*) Origin centroid map for MCM-68 based on one reflection, 520, with $|U_{\mathbf{h}}|^{\rm obs} = 0.19$, $\varphi = 0$. The Si sites are indicated with crosses. (*b*) The centroid map for MCM-68 based on the origin-defined reflections and eight reflections with permuted phases filtered *via* the $P(\delta q)$ function. This is the map with the highest associated likelihood.

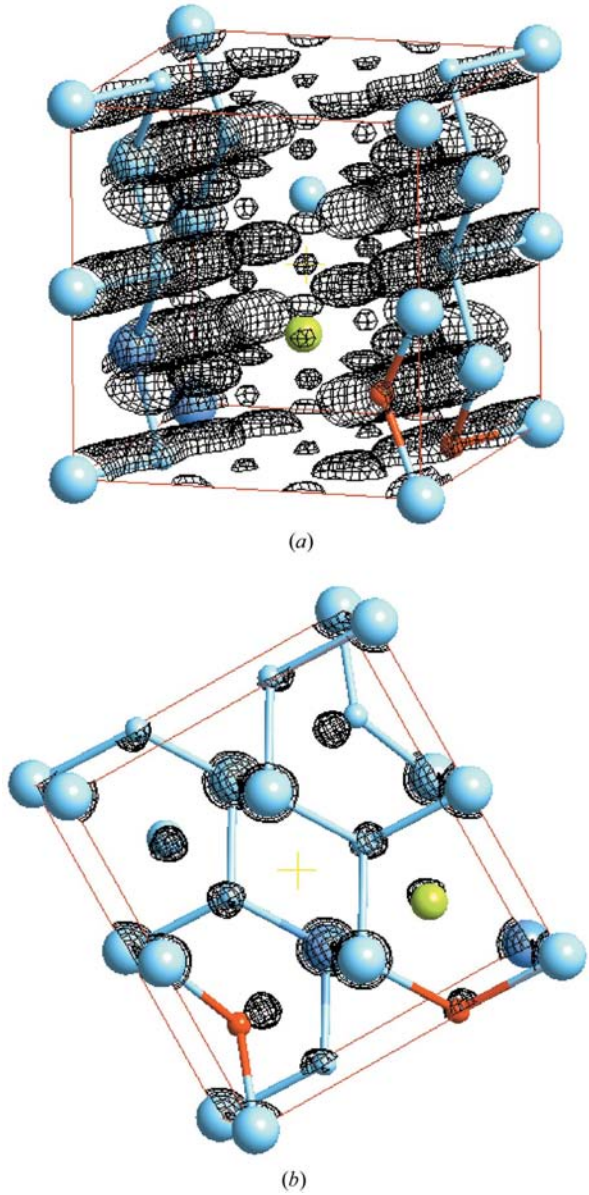

Figure 4
(*a*) Origin map for basic copper chloride, $CuCl_2 \cdot 3Cu(OH)_2$, based on three reflections, 221, 321 and 111, with $|U_{\mathbf{h}}|^{\rm obs} = 0.51$, 0.59 and 0.33, respectively, and with zero phase angles. (*b*) The third-ranked node from LLG calculations following the use of the $P\delta(q)$ function and entropy maximization.

were calculated and analysed. The centroid map from the node with the highest LLG value is shown in Fig. 1(*b*) with the correct Si sites indicated by crosses. The Si-atom framework is clearly identified and all atoms are close to maxima in the map.

3.2. ZSM-5

ZSM-5 (Kokotailo *et al.*, 1978) crystallizes in space group *Pnma* and the data comprise 50 *h*0*l* reflections with a maximum resolution of *ca* 2 Å. The overall temperature factor from normalization was imposed as 4.0 Å^2 since Wilson's method gave a negative overall temperature factor. The origin was defined *via* two reflections, 403 with $|U_{\mathbf{h}}|^{\rm obs} = 0.19$, $\varphi = \pi$, and 503 with $|U_{\mathbf{h}}|^{\rm obs} = 0.16$, $\varphi = 0$. The resulting maximum-entropy map is shown in Fig. 2(*a*). It can be seen that much of the density approximately defines a low-resolution structure but with some spurious peaks. There is sufficient dynamic range in the map for the $P(\delta q)$ formalism to work.

Eight reflections were given permuted phases in a full factorial design. The $P(\delta q)$ function was calculated for each of the 256 phase combinations. The 64 phase sets with the minimum associated values of $P(\delta q)$ were retained and subjected to entropy maximization. The resulting likelihood estimates were calculated and analysed. The top-ranked map *via* LLG estimation is shown in Fig. 2(*b*) with the correct Si sites indicated by crosses. There is one spurious peak at *ca* (0.09,0.78) and Si(2) is only weakly indicated but otherwise the Si-atom framework is clearly identified and atoms are within 0.6 Å of the maxima in the map.

3.3. MCM-68

MCM-68 (Dorset *et al.*, 2006) crystallizes in space group $P4_2/mnm$ and these data comprise 42 *hk*0 reflections with a maximum resolution of *ca* 1.8 Å. Fig. 3(*a*) shows the origin centroid map based on one reflection, 520, with $|U_{\mathbf{h}}|^{\rm obs} = 0.19$, $\varphi = 0$. Fig. 3(*b*) shows the centroid map based on the origin-defining reflections and eight reflections with permuted phases filtered *via* the $P(\delta q)$ function. This is the map with the highest associated likelihood estimate. Two of the *T*-sites are not clearly defined and the problem in which a single elongated peak represents two Si atoms is evident here, and is a consequence of data resolution and sparsity.

3.4. Basic copper chloride

Basic copper chloride, $CuCl_2\cdot 3Cu(OH)_2$ (Voronova & Vainshtein, 1958), crystallizes in space group $P2/m$ and these data comprise 120 reflections with a maximum resolution of *ca*

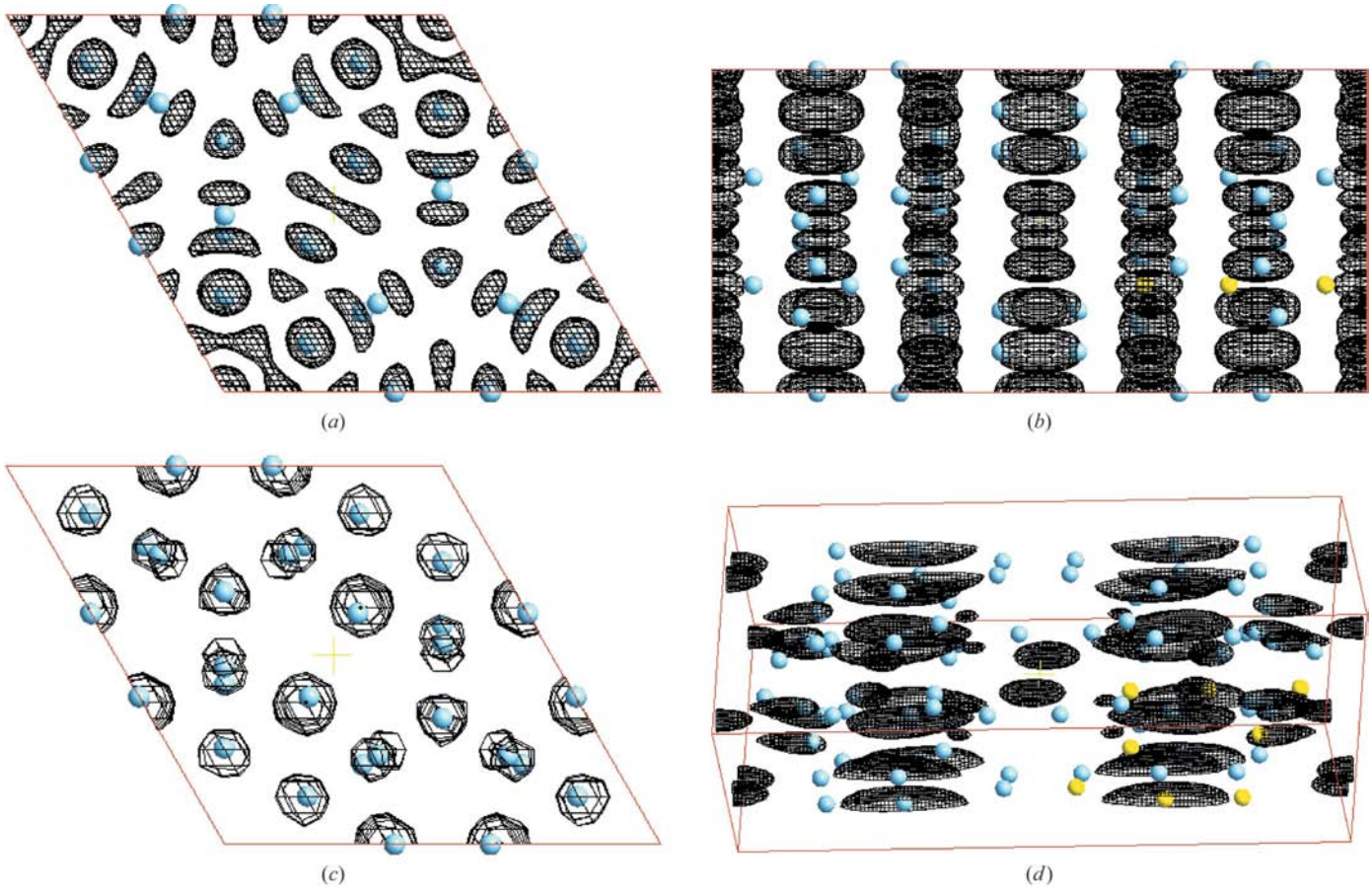

Figure 5
Origin centroid map for MWW based on one reflection, $52\bar{3}$, with $|U_{\mathbf{h}}|^{\rm obs} = 0.24$, $\varphi = \pi$. The Si sites are indicated by spheres. The yellow spheres are the asymmetric unit and the blue ones the symmetry equivalents. (*a*) Looking down the *c* axis and (*b*) looking down the *a* axis. (*c*) Centroid map for node ranked third by LLG analysis following the standard density-building procedure; the map is viewed down the *c* axis, and (*d*) viewed down the *a* axis.

0.7 Å. It is obviously not a zeolite but it is interesting to see if the same principles can be used for inorganic structures. The data set is three dimensional. Normalization included the entire unit-cell contents. Fig. 4(*a*) shows the origin map based on three reflections, 221, 321 and 111, with $|U_{\mathbf{h}}|^{\rm obs} = 0.51$, 0.59 and 0.33, respectively, and with zero phase angles. Fig. 4(*b*) is the centroid map from the third-ranked node from LLG calculations following the use of the $P(\delta q)$ function and entropy maximization. The map is clear and all the atoms except the Cl^- ions are easily located including the O atoms.

3.5. MWW

MWW (Camblor *et al.*, 1998) crystallizes in space group *P*6/*mmm*; this data set comprises 155 reflections with a maximum resolution of *ca* 1.3 Å. It is three-dimensional. Figs. 5(*a*) and 5(*b*) show two views of the origin centroid map based on one reflection, $52\bar{3}$, with $|U_{\mathbf{h}}|^{\rm obs} = 0.24$, $\varphi = \pi$. The Si sites are indicated with spheres. The yellow spheres define the asymmetric unit and the blue ones the symmetry equivalents. The standard density-building procedure was applied. All the top five maps ranked using LLGs were interpretable when viewed down the *c* axis, but the third ranked was the clearest. Figs. 5(*c*) and 5(*d*) show the centroid map for this node. In projection down the *c* axis (Fig. 5*c*), the map is very clear. However, the *a* projection (in Fig. 5*d*) is poor with no interpretable peaks. No other node in the top five as assessed by LLG value was interpretable either. As described in a previous paper (Dorset *et al.*, 2005), this is a consequence of the missing cone of data arising from tilt sampling along $\mathbf{c}^*$, and the structure is best solved in two stages: the two-dimensional projection down **c**, followed by phase extension into the third dimension, but this is beyond the scope of this paper. We are also currently investigating methods of mitigating the missing cone problem using image processing methods used in other fields; these include spectral analysis and the singular-value-decomposition techniques (see, for example, Hansen *et al.*, 2006) and these will be described in a later paper.

3.6. ITQ-29

Given the simplicity of the structure, with one *T*-site in the asymmetric unit, it is surprisingly difficult to solve from this data set. ITQ-29 (LTA) (Reed & Breck, 1956; Corma *et al.*, 2004) crystallizes in space group $Pm\bar{3}m$ and these data comprise 71 reflections with a maximum resolution of *ca* 1 Å. Because the space group is cubic, the data are, in part, three-dimensional although incomplete. An origin was defined using the 111 reflection; the corresponding map is shown in Fig. 6(*a*). The routine application of the density-building method produced poor maps when ranked by LLG. However, it is possible to employ potential-density histograms as figures of merit, as described in detail in the previous paper. When this was done, a node that was poorly ranked by LLG (27th) but ranked second, third and second using the Pearson, Spearman and mean-histogram correlation coefficients (Barr *et al.*, 2004), respectively, gave a map shown in Fig. 6(*b*). There is a spurious peak but the framework is relatively clear.

3.7. ZSM-10

ZSM-10 (Foster *et al.*, 2005; Dorset, 2006) crystallizes in space group *P*6/*mmm* and this data set comprises 29 *hk*0 reflections with a maximum resolution of *ca* 2.7 Å. In this space group with *hk*0 data only, there are no origin-defining reflections, so it would appear that this method would not

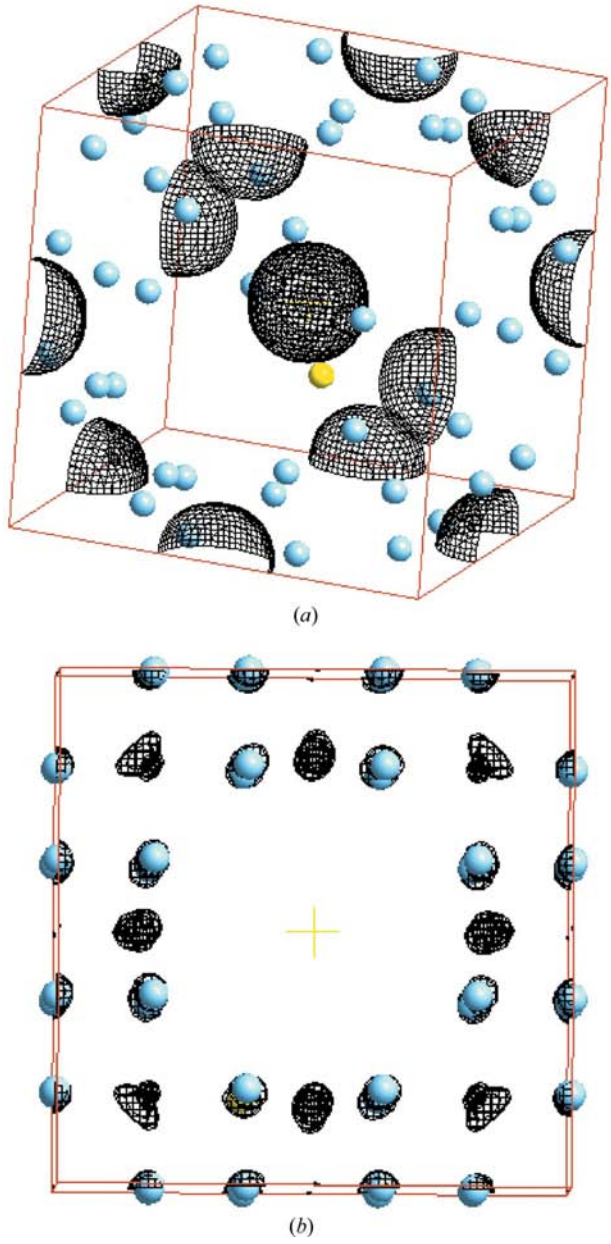

Figure 6
Origin centroid map for ITQ-29 in projection based on one reflection, 111, with $|U_{\mathbf{h}}|^{\rm obs} = 0.38$, $\varphi = 0$. (*b*) A projection for node 21. This is poorly ranked using LLGs (27th) but it is ranked second, third and second using the Pearson, Spearman and mean-histogram correlation coefficients, respectively. The yellow sphere is the single *T* atom found within the asymmetric unit and the blue spheres are symmetry equivalents. (Sometimes the yellow sphere is obscured by the direction of view.)

work in these circumstances. However, there is an alternative strategy. Two reflections were chosen using the same criteria as used for origin definition, but they were given permuted phases instead of fixing them, thus generating four nodes, each of which were subject to entropy maximization. We now have four possible 'origin' maps. The density-building method was applied to each of these four nodes in turn, the results were pooled into one set of 256 nodes (4×64) and analysed together. The solution ranked second *via* LLG is shown in Fig. 7(*a*). The pore is well defined, but atom Si(5) is not visible on the maps. As an experiment, this map was used as the source of $q^{\rm ME}(\mathbf{x})$ for further density building in which eight more reflections were given permuted phases, and used to compute $P(\delta q)$, with subsequent filtering and entropy maximization. The map with the highest LLG value is shown in Fig. 7(*b*). The position of atom Si(5) is now indicated. It was not possible to continue this process because there were insufficient strong reflections.

3.8. ITQ-7

There is a potential problem with this methodology that is exemplified by this data set. ITQ-7 (Villaescusa *et al.*, 1999) crystallizes in space group $P4_2/mmc$ and these data comprise 32 *hk*0 reflections with a maximum resolution of *ca* 1.6 Å. The origin map generated from one reflection 030 with $|U_{\mathbf{h}}|^{\rm obs} = 0.19$, $\varphi = 0$, is shown in Fig. 8(*a*). Two equal areas of density can be seen: one where atom sites are present and one where the converse is true. This latter area runs round the perimeter of the unit cell. In applying the density-building function to this situation, density is built in the wrong place. Fig. 8(*b*) shows a typical example: only the coordinates of Si(1) are correctly indicated but the map is wrong and uninterpretable. A possible way to alleviate this problem is to incorporate prior

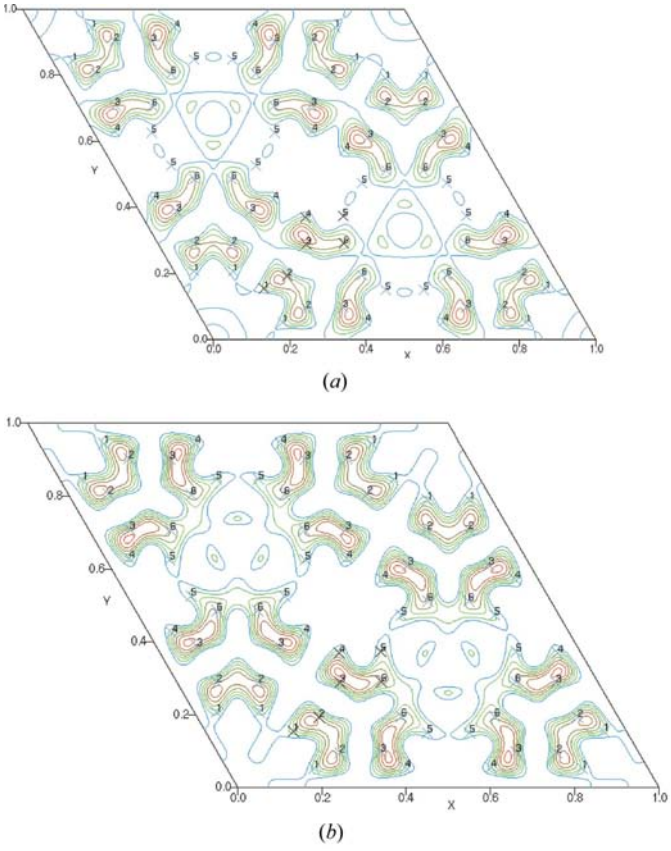

Figure 7
The second-ranked map using LLG estimates for ZSM-10. (No origin map is possible with these data and space group.) All the other top five nodes showed only one large peak at the unit-cell origin. (*b*) The result of further density building on this node. Eight more weak reflections have been included in the basis set.

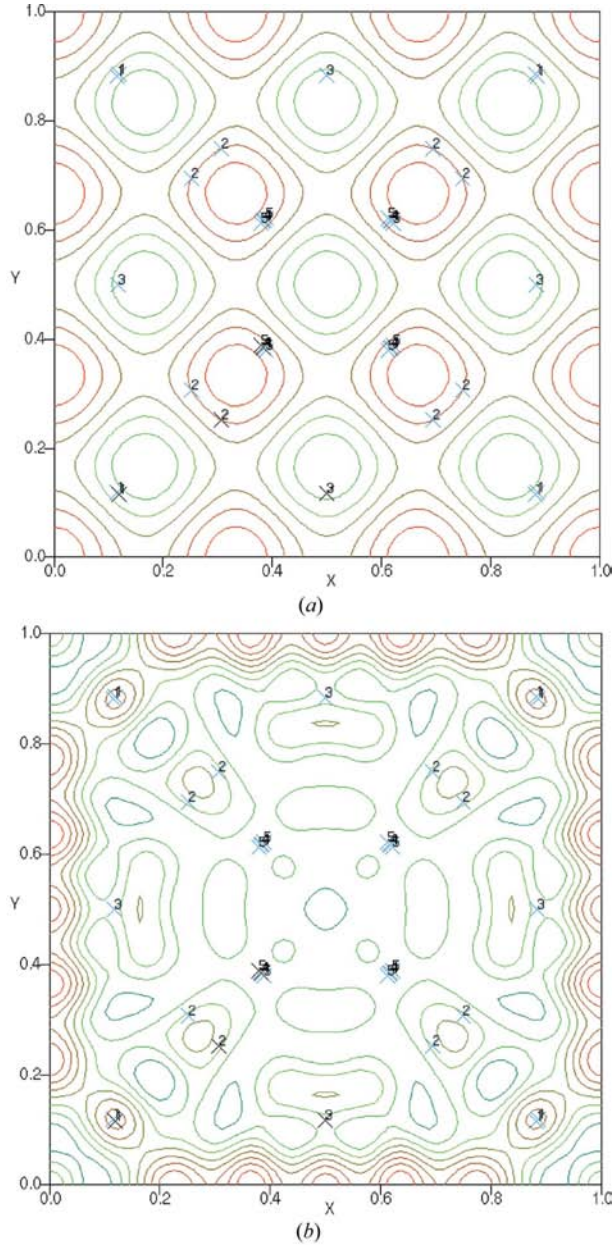

Figure 8
Origin centroid map for ITQ-7 based on one reflection, 030, with $|U_{\mathbf{h}}|^{\rm obs} = 0.19$, $\varphi = 0$. The Si sites are indicated with crosses. High density is red, low density is green. (*b*) Typical centroid map based on the origin-defining reflections plus eight reflections with permuted phases filtered *via* the $P(\delta q)$ function. The density has been built in the wrong region and the structure is not solved.

knowledge of the pore size into the methodology and we are currently investigating this possibility. The ME method allows the incorporation of such data in an easy and natural manner but it lies beyond the scope of this paper.

4. Conclusions and further developments

We have presented a method of solving zeolite structures from electron diffraction data using maximum-entropy and likelihood methods supplemented with a density-building function that enhances the sampling of phase space when compared to the use of likelihood alone. Since the method needs Fourier maps in which the use of origin reflections only can generate useful information, the method is well suited to these structures as the unit-cell contents are relatively small and the U magnitudes large. The method is very fast: the computer time needed on a modest PC running at 2.8 GHz with 1 Gbyte of RAM and running Windows XP was never more than 2 min. The only caveat is the problem that arose with ITQ-7 in which density, given the choice of two areas in which to build, preferentially builds in the wrong zone, but this happened only once in eight trials. It has also been successful in the solution of an inorganic copper salt. The method is also capable of being combined in an automatic way with histogram matching, and we are working towards this goal in the *MICE* program.

There are some exciting possibilities for extending this work.

1. The use of prior information of pore size and position: this can come from electron microscopy, simulation studies or comparison with known frameworks. The pore then becomes a prior $m(\mathbf{x})$ and this is used throughout the calculation as a modifier to $q^{\rm ME}(\mathbf{x})$ (Bricogne, 1984). For example, the density-building function now takes the form

$$P(\delta q) = \int_V \frac{\delta q(\mathbf{x})^2}{m(\mathbf{x}) q^{\rm ME}(\mathbf{x})}\,{\rm d}\mathbf{x}. \qquad (3)$$

2. The use of fragments: given a series of possible maps, it is useful to choose potential atomic peaks on the basis of not only geometry but also using entropy and likelihood considerations with their generally robust behaviour with respect to data errors. In this case, we can use not only $|U_{\mathbf{h}}|^{\rm obs}$, $|U_{\mathbf{h}}|^{\rm ME}$ and their associated phase angles, but also $|U_{\mathbf{h}}|^{\rm frag}$ calculated from the proposed fragment and its phase angle. These three U magnitudes are suitably scaled. We are currently testing this methodology to both validate and complete zeolite structures.

3. Equation (2) is not the only available density-building function. For example, we can use

$$P(\delta q^2) = -\int_V \frac{[\delta q(\mathbf{x})]^3}{[q^{\rm ME}(\mathbf{x})]^2}\,{\rm d}^3\mathbf{x}. \qquad (4)$$

4. This function has only been examined in relation to protein structure solution (Tate, 2003), where it showed some promise. It may prove to be a useful auxiliary function used with or without pore information. It can be calculated at the same time as $P(\delta q^2)$ without any significant extra computation time required.

Methods 1–3 are not mutually exclusive but can be used in combination with every prospect of improving our capabilities in electron crystallography.

CJG acknowledges support from ExxonMobil Research and Engineering Co. and the University of Glasgow.

References

Barr, G., Dong, W. & Gilmore, C. J. (2004). *J. Appl. Cryst.* **37**, 243–252.
Bricogne, G. (1984). *Acta Cryst.* A**40**, 410–445.
Bricogne, G. & Gilmore, C. J. (1990). *Acta Cryst.* A**46**, 284–297.
Camblor, M. A., Corma, A., Diaz-Cabanas, M.-J. & Baerlocher, C. (1998). *J. Phys. Chem. B*, **102**, 44–51.
Corma, A., Rey, F., Rius, J., Sabater, M. J. & Valencia, S. (2004). *Nature (London)*, **431**, 287–290.
Dorset, D. L. (2006). *Z. Kristallogr.* **221**, 260–265.
Dorset, D. L., Roth, W. J. & Gilmore, C. J. (2005). *Acta Cryst.* A**61**, 516–527.
Dorset, D. L., Weston, S. & Dhingra, S. S. (2006). *J. Phys. Chem.* **110**, 2045–2050.
Foster, M. D., Treacy, M. M. J., Higgins, J. B., Rivin, I., Balkovsky, E. & Randall, K. H. (2005). *J. Appl. Cryst.* **38**, 1028–1030.
Gilmore, C. J. & Bricogne, G. (1997). *Methods in Enzymology*, edited by C. W. Carter Jr & R. M. Sweet, pp. 65–78. New York: Academic Press.
Gilmore, C. J., Bricogne, G. & Bannister, C. (1990). *Acta Cryst.* A**46**, 297–308.
Gilmore, C. J., Dong, W. & Dorset, D. L. (2008). *Acta Cryst.* A**64**, 284–294.
Gilmore, C. J., Henderson, K. & Bricogne, G. (1991). *Acta Cryst.* A**47**, 830–841.
Gilmore, C. J., Shankland, K. & Fryer, J. (1993). *Ultramicroscopy*, **49**, 132–146.
Golay, M. J. E. (1949). *Proc. IEEE*, **37**, 23–28.
Hansen, B. C., Nagy, J. G. & O'Leary, D. P. (2006). *Deblurring Images. Matrices, Spectra and Filtering.* Philadelphia: Society for Industrial and Applied Mathematics.
Henderson, K. & Gilmore, C. (1989). *Maximum Entropy and Bayesian Methods*, edited by J. Skilling, pp. 233–239. Dortrecht: Kluwer Academic Publishers.
Kokotailo, G. T., Lawton, S. L., Olson, D. H. & Meier, W. M. (1978). *Nature (London)*, **272**, 437–438.
Meier, W. M. (1961). *Z. Kristallogr.* **115**, 439–450.
Reed, T. B. & Breck, D. W. (1956). *J. Am. Chem. Soc.* **78**, 5972–5977.
Rogers, D. (1980). *Theory and Practice of Direct Methods in Crystallography*, edited by M. F. C. Ladd & R. A. Palmer, pp. 23–92. New York: Plenum Press.
Shankland, K., Gilmore, C. J., Bricogne, G. & Hashizume, H. (1993). *Acta Cryst.* A**49**, 493–501.
Tate, G. (2003). PhD thesis, University of Glasgow, UK.
Villaescusa, L. A., Barrett, P. A. & Camblor, M. A. (1999). *Angew. Chem. Int. Ed.* **38**, 1997–2000.
Voronova, A. A. & Vainshtein, B. K. (1958). *Sov. Phys. Crystallogr.* **3**, 445–451.